solids

MDPI

Article

Contactless Determination of Electric Field in Metal–Insulator–Semiconductor Interfaces by Using Constant DC-Reflectivity Photoreflectance

Eiichi Kobayashi [1,*], Koya Satta [2], Ryoga Inoue [2], Ken Suzuki [2] and Takayuki Makino [3]

[1] Advanced Interdisciplinary Science and Technology, Graduate School of Engineering, University of Fukui, Fukui 910-8507, Japan
[2] Department of Electric and Electronics Engineering, University of Fukui, Fukui 910-8507, Japan; hb170548@u-fukui.ac.jp (K.S.); hb170122@u-fukui.ac.jp (R.I.); mf200781@u-fukui.ac.jp (K.S.)
[3] Research Center for Development of Far-Infrared Region, University of Fukui, Fukui 910-8507, Japan; tmakino@u-fukui.ac.jp
* Correspondence: ei-koba@u-fukui.ac.jp

Abstract: We applied photoreflectance (PR) spectroscopy for contactless determination of the electric field strength at buried interfaces in metal–insulator–semiconductor (MIS) structures. The PR is an all-optical version of an electromodulated reflectance spectroscopy. The tradeoff of this adoption is that this requires an additional feedback system to eliminate background problems induced by scattered pump light and/or photoluminescence. A microcomputer-based feedback system has been developed for this elimination. Despite the very tiny signal intensity, we successfully attained a sufficiently good signal–noise ratio to determine the electric field strength in oxide-based MIS interfaces that exhibits a large, unwanted photoluminescence signal. The field strength was evaluated to be ca. 0.25 kV/cm.

Keywords: optical properties; interface science; instrumentation

Citation: Kobayashi, E.; Satta, K.; Inoue, R.; Suzuki, K.; Makino, T. Contactless Determination of Electric Field in Metal–Insulator–Semiconductor Interfaces by Using Constant DC-Reflectivity Photoreflectance. *Solids* **2021**, 2, 129–138. https://doi.org/10.3390/solids2020008

Academic Editors: Michael Reshchikov and Joaquim Carneiro

Received: 11 February 2021
Accepted: 21 March 2021
Published: 29 March 2021

1. Introduction

Modulation spectroscopy has played an important role in characterizing the optical properties of solids [1–4]. Due to its inherent derivative nature, the resultant spectrum becomes free from the broad background [5]. This spectroscopy has been mainly used for an electronic-band-structure characterization. As stated explicitly by Aspnes and coworkers [1,2], the electroreflectance (ER) can also detect, in principle, the Franz–Keldysh oscillation (FKO) as a result of the relatively strong built-in electric field despite its signal intensity—at least one order of magnitude smaller than the band-edge response [6–8].

Photorefletance (PR) is known to be one of such modulation spectroscopies [3,4]. Traditionally, external perturbations such as electric fields have been applied to measure differential reflectivity. In the case of PR, perturbation is implemented through an additional pump laser beam by modulating the built-in electric fields near the solid surfaces. Photo-absorbed electrons are excited, and the dielectric constant is resultingly changed in accordance with the change of the electronic distributions. Then, the change in the dielectric constant induces the change of the reflectivity. This spectroscopy has desirable attributes such as its non-destructive and contactless properties [9,10]. These are attractive for the contactless assessment of the interface properties such as electric field strength and Schottky barrier height because of its possibility of extension to the in situ diagnosis, which is compatible with the processing environments [11,12]. It should be noted that it is very difficult to accomplish in the cases of other kinds of contactless probes [13–15].

On the other hand, the PR has a drawback that is well-known as "the spurious signal problem" [16–18]. This is owing to the interfusion with photoluminescence (PL) or laser scattered light. Due to this, the detection limit of this spectroscopy seems to be

worse than that of the ER spectroscopy. A look through the literature revealed that many works related to the detection of the FKO in wide-gap semiconductors have been mainly dedicated to multiple quantum wells, where the signal intensity was earned with the periodicity of the structures [19]. There are few works except for that in Au Schottky contacts on GaN [20]. A contactless characterization tool should preferably cover the basic device structures such as bulk-crystalline-based Schottky diodes and simple metal–insulator–semiconductor (MIS) structures. To suppress the spurious contribution and to enhance the detection limit, Shen and coworkers [16] proposed keeping the direct current (DC) component (V_{dc}) constant independent of the photon energy, enabling the facile a posteriori subtraction of the spurious signal contributions [17]. While this was originally termed a new normalization procedure, we rather call it a constant DC-reflectivity PR, in analogy with the constant photocurrent method [21]. Among many other methods previously proposed, this technique can most soundly balance between advantages and cost-effectiveness [18,22–24].

This paper describes a microcomputer-based implementation of the constant DC-reflectivity PR spectroscopy because obsolete electrical parts adopted in the original work [16] must have been replaced with the state-of-the-art counterparts. After explaining the design of our feedback system, we demonstrate how to efficiently maintain the constant DC component voltage (V_{dc}) with this. Finally, we report our observation of FKO in the PR spectrum taken for an oxide-based MIS structure that exhibits a large, unwanted PL signal. The interface electric field strength is also evaluated.

2. Experimental Procedures

As earlier stated, it is considered to be very difficult to detect tiny FKO-related signals without the extension to the conventional PR. This is especially true for the widegap-semiconductor-based simple Schottky or MIS diodes. It is impossible to reproduce the original set-up [16] with the electrical parts available nowadays. Therefore, let us explain our system in detail.

First, we explain why we normalized the DC reflectivity (V_{dc}) for the PR for the spurious signal suppression. Signals detected with the modulation spectroscopy include two components; i.e., V_{dc} and modulated AC components (V_{ac}) [16]. The quantity that we wish to obtain is V_{ac} divided by V_{dc}. A detailed explanation of the principle can be found elsewhere [16,23]. We only show the relevant equations below without introducing excessively complicated quantities. By letting E take photon energy, the DC output can be expressed as:

$$V_{dc} = I_0 R(E). \tag{1}$$

Here, I_0 denotes an effective input intensity that also accounted for gains of the avalanche photodetector (APD) and post-amplifier. In other words, I_0 is an inputting intensity multiplied by these gains.

On the other hand, spurious signals tend to contribute to the V_{ac} in PR, and this reads:

$$V_{ac} = I_0 \Delta R(E) + I_{sp}, \tag{2}$$

where I_{sp} denotes the intensity of spurious component that includes again the abovementioned gains. It should be noted that I_{sp} is independent of the photon energy because of the dark configuration. In other words, this can be regarded as a constant.

Thus, the relationship between V_{dc}/V_{ac} and $\Delta R/R$ can be written as

$$\frac{V_{dc}}{V_{ac}}(E) = \frac{I_0 \Delta R(E) + I_{sp}}{I_0 R(E)} = \frac{\Delta R(E)}{R(E)} + \frac{I_{sp}}{V_{dc}}. \tag{3}$$

The second term of Equation (3) becomes constant if the $V_{dc}(E)$ is independent of probe energy (E). That is why we wish to keep the V_{dc} irrespective of the photon energy. This facilitates an a posteriori subtraction of the spurious signal.

In the original approach [16], a variable neutral density filter (VNDF) mounted on a servo-motor was adopted to maintain constant V_{dc}. A VNDF is a filter that allows you to adjust the attenuation of the incoming light intensity. By rotating the filter, the filter shifts between low and high attenuations. The basic design of the servo-motor-based control system is shown in Figure 1. It is known that the precision in position determination of a stepping motor is superior to that of the servo motor. However, the control requirements of the stepping-motor drive are so unique that the concepts for the servo motors can hardly be extrapolated to those of the stepping motors. A driver for a stepping motor is usually controlled with a personal computer (PC), which tends to severely deteriorate the stability of the feedback systems due to the power-line noise. On the other hand, if this is controlled with a low-cost RISC (reduced instruction set computer) microcontroller, i.e., Arduino ATmega328P, it also enables stability attainable with the battery power feeding.

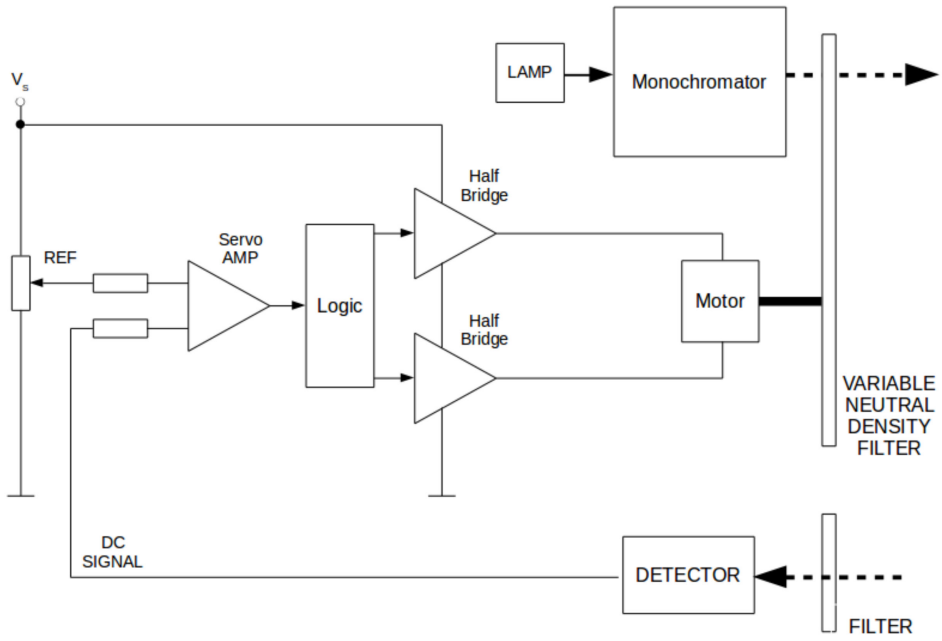

Figure 1. A block diagram showing the basic design of the analog servo-motor-based feedback system.

Next, we explain our proposed designs on the algorithm and circuits for the stepping motor drive system, which is power-delivered from the DC batteries, as shown in Figure 2. We drove this stepping motor by using a stage controller (PAT-001, Sigma Koki Co. Ltd., Tokyo, Japan). The power driving source is a lead-acid battery. We developed an original circuit for the RISC control. For the feedback, the pulse number sending to the stepping motor was adjusted following the distance between the present and target values (otherwise known as V_{dc}) [25].

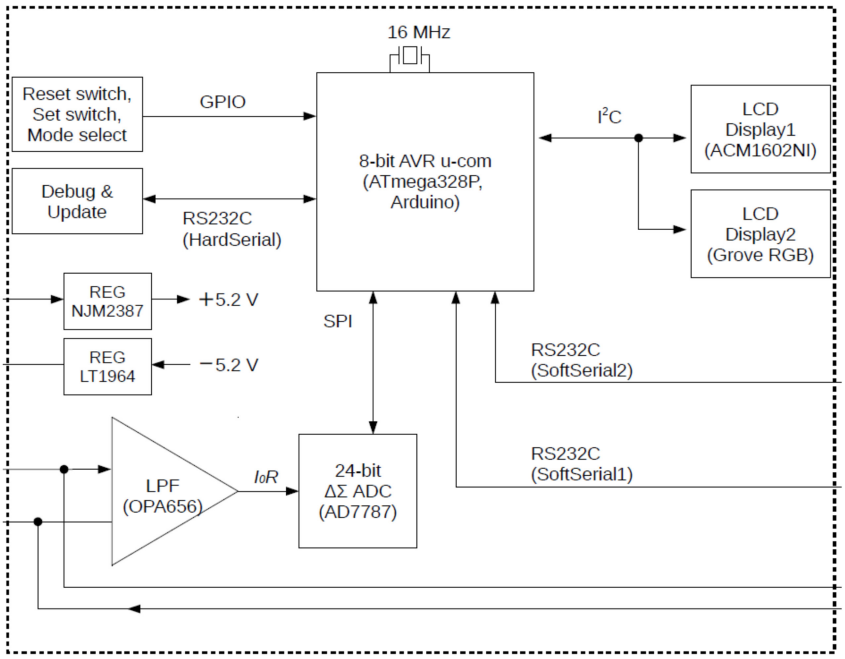

Figure 2. A block diagram showing the proposed design on our microcomputer-based system. The list of abbreviations is as follows: LCD: liquid crystal display, APD: avalanche photodiode, AMP: amplifier, LPF: low-pass filter, VNDF: variable neutral density filter, REG: voltage regulator, and ADC: analog–digital converter. Nomenclatures of ATmega328P (RISC (reduced instruction set computer) controller), APD440A2, OPA656, and AD7787 are the product numbers.

Next, we describe the algorithm of our proposed design. Figure 3 shows a flow chart of our feedback system. We used the Arduino language, which is similar to the C/C++ language, for coding. As shown in the right-hand side panel of Figure 3, we determined the sign of the number of pulses, depending on the positive/negative in the difference between current DC reflectivity and the target V_{dc}. Additional care has to be taken if an APD is used as a detector instead of a photo-multiplier tube. As shown in Figure 4, there is a relatively large variation in its sensitivity curve especially in the UV range. As earlier stated, our main target is related to the wide-gap semiconductors. Therefore, we decided on mutual communication between the RISC and the monochromator. To minimize the influence of the PC noise, we used a universal photocoupler (TLP785) and added an isolated communication circuit to the communication path between the VNDF control unit and a PC. We ensured electrical isolations between the VNDF and the PC, while the bidirectional communication was implemented. We set the baud rate down to 1200 bps (bit per second) to avoid unfaithful waveform transform and the resulting communication errors. As shown on the left-hand side of Figure 3, the RISC controller inquires about the current photon energy before calling the subroutine for the feedback control. Then, we calculate the absolute number of the pulse sending to the motor by introducing two following empirical parameters, i.e., k and lum, respectively. Since the sensitivity of the APD significantly depends on the photon energy, the V_{dc} change per the density-filter angle also depends on the energy. The parameter k takes this effect into account. Then, we divided the sensitivity curve of the APD into five regions, as shown by the vertical lines in Figure 4. We have performed the linear regression analysis for each region to determine the slopes. The value of k was finally calculated from the absolute value of the slopes of the sensitivity curve. To avoid the so-called overshooting behavior, we introduced an additional empirical parameter lum. This parameter was decided by the difference between the current value and the target V_{dc}. The adjustment method of this parameter is similar to the parameter p in the PID (proportional–integral–derivative) language. By accounting for the above-mentioned parameters, we calculated the number of pulses (N_{puls}) according

to the equation: $N_{\mathrm{puls}} = k \times lum$. It should be noted that we rounded N_{puls} to make the number integer only. We repeated such feedback until the convergence. The convergence was judged if the difference falls within acceptable limits, i.e., $\pm 1\%$ of the target V_{dc}. In the case of the APD PR spectroscopy for the near UV region, our algorithm allowed us to result in more secure convergence rather than the use of the PID subroutine equipped by the Arduino library.

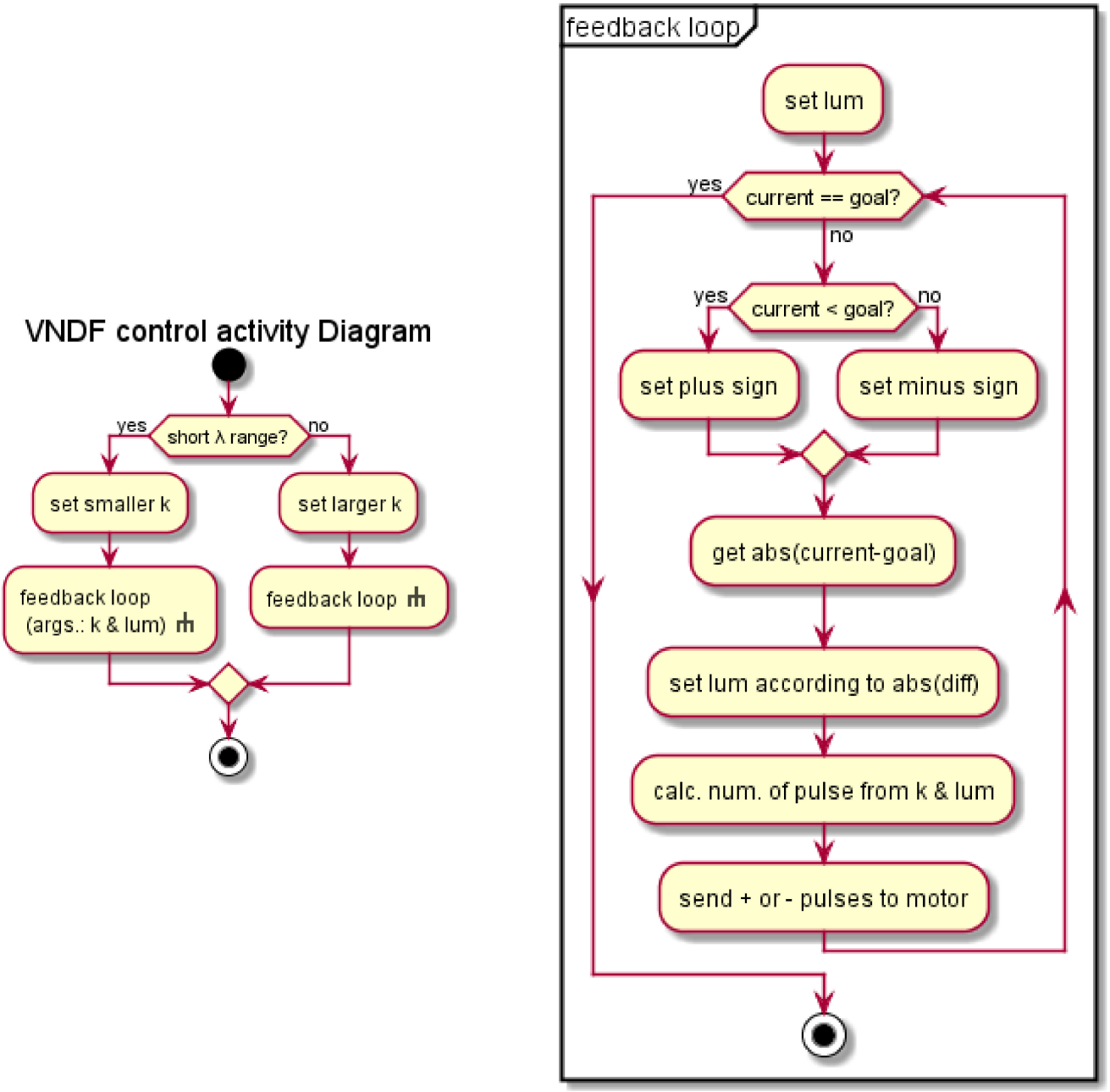

(**a**) (**b**)

Figure 3. A flow chart showing the main parts of the feedback algorithm (**a**) with the called sub-routine (**b**). The name of the sub-routine is feedback loop. For the want of space, the number of the energetic (wavelength) regions was limited to two regions, although the actual number of the regions was five. The symbol λ depicts the wavelength (energy) of the detection. The flow chart only concerns the communication between the motor-driver and the RISC. Values of k and lum are related to the weights used to determine the number of the pulses sent to the stepping motor. Arguments were abbreviated as "args" here.

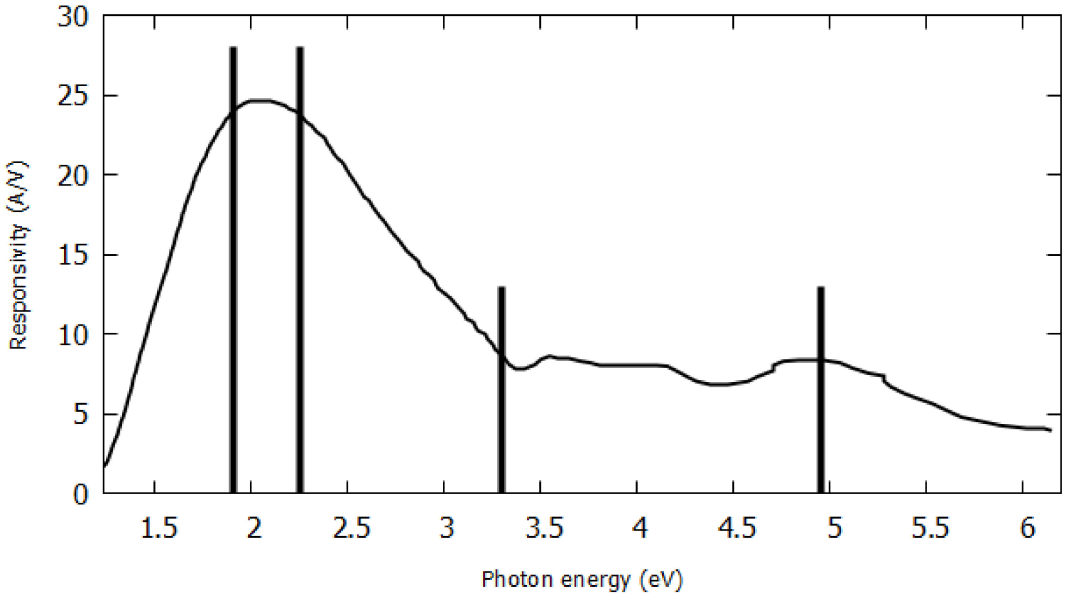

Figure 4. Sensitivity curve of avalanche photodiode. Four vertical lines separates the five energetic regions to control our feedback system.

Finally, we explain our optical set-up and device under test (DUT). We adopted what is often called a dark configuration, i.e., the monochromatized probe beam fed onto the DUT. As a chopped pump beam, we used 325-nm-line from an HeCd laser. The reflected probe beam was focused on the APD. Irises were placed in our optical path to limit the acceptance angle [26]. While the PL angular distribution follows Lambert's cosine law, the directionality of the reflectance is superior to that of PL. The iris insertion technique can block the PL signals, thereby drastically reducing the collection efficiency of PL signals, i.e., the spurious contribution. As long as an Xe arc lamp is used as a probe source, this technique is not sufficient to completely suppress the spurious contribution. Despite its incompleteness, this helped the efficiency and precision of our constant DC-reflectivity PR. The DUT is a ZnO-based MIS structure. We introduced additional stacking layers of several-nm-thick Al_2O_3 and semitransparent gold on a commercially available ZnO crystal using the atomic layer deposition technique. The DUT was attached to a cold finger of a refrigerator for cryogenic temperature measurement.

3. Experimental Results and Discussion

Figure 5 shows the $V_{dc}(E)$ spectra with using the VNDF control. The target V_{dc}s are 300, 750, 1000, 2500, and 3500 mV, respectively. As can be understood from Figure 5, it can be said that we successfully control the feedback with the various V_{dc} values. Moreover, this control system attained good performance on reproducibility.

Having established our PR scheme, we measured a PR spectrum for the ZnO-based MIS structure [27,28]. Figure 6 shows the differential reflectivity spectrum (closed circles) using the VNDF. The measurement temperature is approximately 180 K. The spurious signal subtraction has been made already to show this datum. A calculated result using Equation (2) of Ref. [29] is shown with a solid line. In addition to the excitonic anomaly (at approximately 3.35 eV), we can also observe an oscillatory structure above this resonance energy [30,31]. This observation suggests a strong-field regime [1,2]. The electric field is concentrated near the interface of this MIS structure [32–34]. The distortion of the PR lineshape from that in the low-field regime suggests that the higher energy signal can be assigned to the FKO [6–8,35–37]. For the analysis, we adopted the theory by Aspnes [1,2], the functional forms of which were concisely formulated in Equation (2) of Ref. [29]. We adjusted the relevant parameters to reproduce the behavior of observed FKO while sacrificing the coincidence around the excitonic anomaly (at 3.35 eV). We believe that the

signal-to-noise ratio here is sufficiently high enough to be able to determine the energies of nodes and antinodes of the FKO. This may be justified if we consider the fact that the FKO signal is generally tiny, especially in the case of the wide-gap semiconductors. The value of V_{dc} for this measurement was 750 mV. While the slight increase in this quantity allowed the observation of the FKO, the distortion of the waveform became severe at the V_{dc} levels greater than 2.5 kV.

Hereafter, we explain how to evaluate the electric field strength from the FKO. From the oscillating period, a parameter Θ was determined to be ca. 0.021 eV. By letting m_e take the electron effective mass, the electric field F is related with Θ through $F^2 = 2m_e\,\Theta^3/(e\hbar)^2$. Nomenclatures other than m_e have their standard meanings. Since the electron mass of ZnO is 0.23 m_0 [38], then the electric field was evaluated to be ca. 0.25 kV/cm, which is in the same order of magnitude as the case of the Schottky contact on GaN. The values are $\Theta \cong 0.04$ eV, and $m_e = 0.22\ m_0$, respectively. It should be noted that the energetic determination of the nodes and antinodes enables the quantification of the electric field strength without the model regression analysis, as has been performed in Ref. [20].

Finally, we mention the discrepancy at the excitonic resonance. Although the reason for this discrepancy is not clear at moment, this is attributed to the fact that the present model is based on the standard-critical-point (SCP) theory. The existence of the strong built-in electric field tends to screen the Coulomb force between an electron and a hole, resulting in an excitonic instability [39]. Probably, such an unstable exciton cannot be correctly modeled in the framework of the SCP model [3–5].

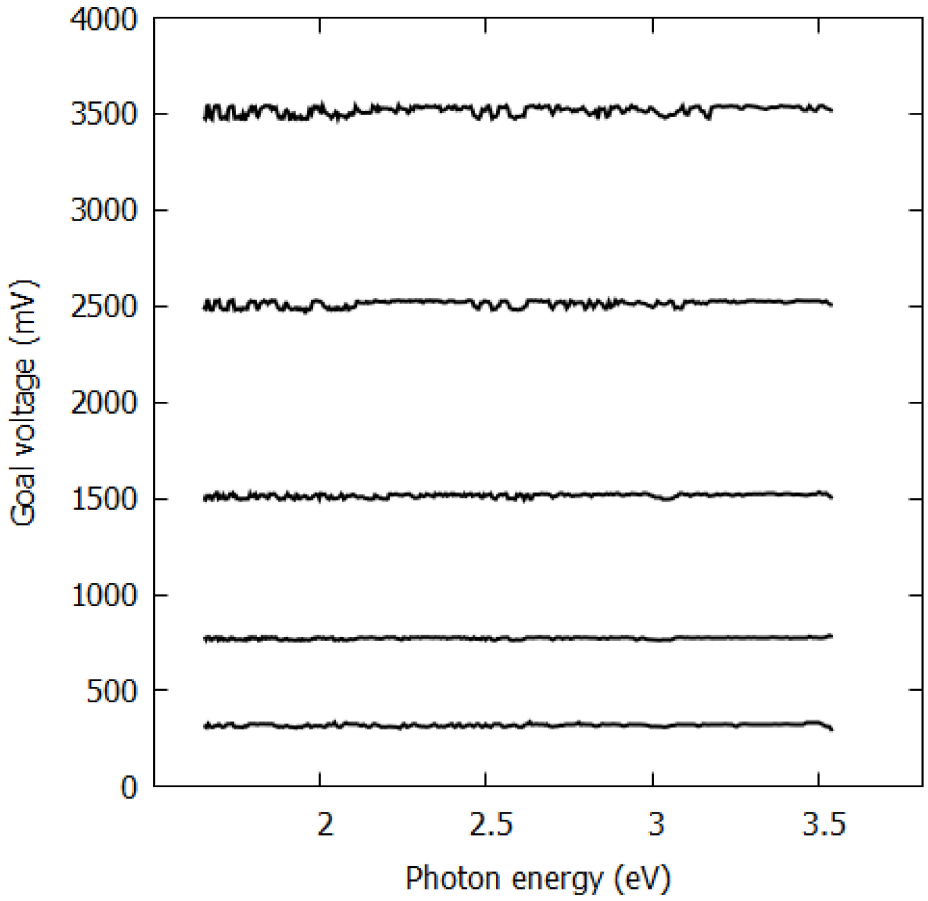

Figure 5. The result of the actual machine test. VNDF-controlled results of the DC component intensity (V_{dc}) are shown as a function of the energy of the probe beam. The system can be adapted for a sufficiently wide range of V_{dc} from 300 to 3500 mV.

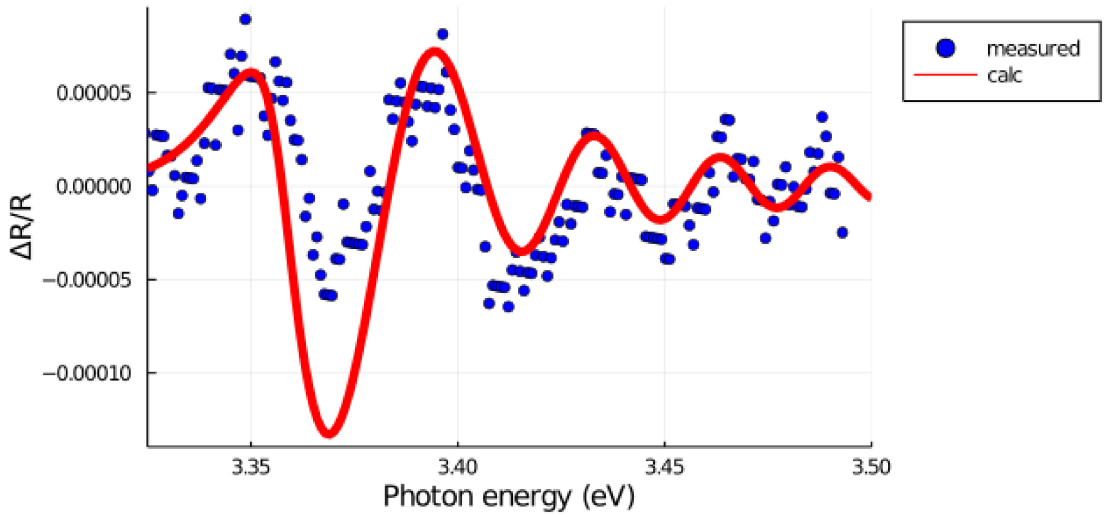

Figure 6. The photoreflectance spectrum of ZnO (closed circles) with using the VNDF. This spectrum is measured at 180 K. The solid line corresponds to a calculated result using Equation (2) of Ref. [29].

4. Conclusions

For the contactless determination of the interface electric field, we have customized PR spectroscopy unaffected by unwanted spurious signals. We describe state-of-the-art electronics implementation to vary the intensity of the probe beam to maintain a constant V_{dc} instead of the traditional servomechanism. This accomplishment provides a cost-effective solution based on microcomputers for constant DC-reflectivity PR spectroscopy. This system can be assembled easily because they consist of versatile electronic parts that are often used in controlling circuits nowadays. The advantage of our method has been demonstrated on a ZnO-based MIS structure that exhibits a large, unwanted PL signal. The electric field strength was also evaluated. It is expected that this can be also applied to the spectroscopies other than the PR such as the constant photocurrent method [21].

Author Contributions: Conceptualization, E.K. and T.M.; methodology, E.K.; software, E.K.; validation, E.K., K.S. (Koya Satta) and K.S. (Ken Suzuki); measurements, K.S. (Koya Satta), R.I., K.S. (Ken Suzuki); writing, T.M., E.K.; visualization, T.M., E.K., K.S. (Koya Satta), R.I.; supervision, T.M.; project administration, T.M.; funding acquisition, T.M. All authors have read and agreed to the published version of the manuscript.

Funding: This research was funded by the Ministry of Education, Culture, Sports, Science and Technology, grant number KAKENHI-19K05303.

Institutional Review Board Statement: Not applicable.

Informed Consent Statement: Not applicable.

Data Availability Statement: The data presented in this study are available on request from the corresponding author. The data are not publicly available due to privacy.

Acknowledgments: Technical assistance from H. Yamamori from the University of Fukui is acknowledged. Atomic layer deposition was performed in Tohoku University, Japan. We acknowledge the permission of its machine time. We acknowledge the scientific contribution from A. Hashimoto (University of Fukui).

Conflicts of Interest: The authors declare no conflict of interest.

References

1. Aspnes, D.E. Third-Derivative Modulation Spectroscopy with Low-Field Electroreflectance. *Surf. Sci.* **1973**, *37*, 418. [CrossRef]
2. Aspnes, D.E.; Studna, A.A. Schottky-Barrier Electroreflectance: Application to GaAs. *Phys. Rev. B* **1973**, *7*, 4605. [CrossRef]
3. Pollak, F.H. Modulation Spectroscopy as a Technique for Semiconductor Characterization. *Proc. SPIE* **1981**, *276*, 142. [CrossRef]

4. Pollak, F.H.; Glembocki, O.J. Modulation Spectroscopy of Semiconductor Microstructures: An Overview. *Proc. SPIE* **1988**, *946*, 2. [CrossRef]
5. Pollak, F.H.; Shen, H. Modulation Spectroscopy of Semiconductors: Bulk/Thin Film, Microstructures, Surfaces, Interfaces and Devices. *Mater. Sci. Eng. R* **1993**, *10*, 275. [CrossRef]
6. Franz, W. Einfluss Eines Elektrischen Feldes Auf Eine Optische Absorptionskante. *Z. Naturforsch.* **1958**, *13a*, 484. [CrossRef]
7. Keldysh, L.V. The Effect of a Strong Electric Field on the Optical Properties of Insulating Crystals. *Sov. Phys. JETP* **1958**, *7*, 788.
8. Ralph, H.I. On the Theory of the Franz-Keldysh Effect. *J. Phys. C* **1968**, *1*, 378. [CrossRef]
9. Qin, J.; Huang, Z.; Ge, Y.; Hou, Y.; Chu, J. Tandem Demodulation Lock-in Amplifier Based on Digital Signal Processor for Dual-Modulated Spectroscopy. *Rev. Sci. Instrum.* **2009**, *80*, 033112. [CrossRef] [PubMed]
10. Yan, D.; Qiang, H.; Pollak, F.H. A New Offset Technique for Suppression of Spurious Signals in Photoreflectance Spectra. *Rev. Sci. Instrum.* **1994**, *65*, 1988. [CrossRef]
11. Acher, O.; Omnes, F.; Razeghi, M.; Drevillon, B. In Situ Characterization by Reflectance Difference Spectroscopy of III-v Materials and Heterojunctions Grown by Low Pressure Metal Organic Chemical Vapour Deposition. *Materials Sci. Eng. B* **1990**, *5*, 223. [CrossRef]
12. Yasuda, T. In Situ Characterization of ZnSe/GaAs Interfaces by Reflectance Difference Spectroscopy. *J. Vacuum Sci. Technol. B Microelectron. Nanometer Struct.* **1996**, *14*, 3052. [CrossRef]
13. Yin, X.; Pollak, F.H. Novel Contactless Mode of Electroreflectance. *Appl. Phys. Lett.* **1991**, *59*, 2305–2307. [CrossRef]
14. Motyka, M.; Kudrawiec, R.; Sek, G.; Misiewicz, J.; Bisping, D.; Marquardt, B.; Forchel, A.; Fischer, M. Contactless Electroreflectance Investigation of Energy Levels in a 1.3 Micron Emitting Laser Structure with the Gain Medium Composed of InAsN Quantum Dots Embedded in GaInNAs/GaAs Quantum Wells. *Appl. Phys. Lett.* **2007**, *90*, 221112. [CrossRef]
15. Lin, H.; Braeuninger-Weimer, P.; Kamboj, V.S.; Jessop, D.S.; Degl-Innocenti, R.; Beere, H.E.; Ritchie, D.A.; Zeitler, J.A.; Hofmann, S. Contactless Graphene Conductivity Mapping on a Wide Range of Substrates with Terahertz Time-Domain Reflection Spectroscopy. *Sci. Rep.* **2017**, *7*, 10625. [CrossRef]
16. Shen, H.; Parayanthal, P.; Liu, Y.F.; Pollak, F.H. New Normalization Procedure for Modulation Spectroscopy. *Rev. Sci. Instrum.* **1987**, *58*, 1429. [CrossRef]
17. Qiang, H.; Yan, D.; Yin, Y.; Pollak, F.H. Characterization of Semiconductor Device Structures by Modulation Spectroscopy. *Proc. SPIE* **1994**, *2141*, 58. [CrossRef]
18. Li, Q.; Tan, H.H.; Jagadish, C. A New Optical Front-End Compensation Technique for Suppression of Spurious Signal in Photoreflectance Spectroscopy Using an Antiphase Signal. *Rev. Sci. Instrum.* **2010**, *81*, 043102. [CrossRef]
19. Wetzel, C.; Takeuchi, T.; Amano, H.; Akasaki, I. Piezoelectric Franz-Keldysh Effect in Strained GaInN/GaN Heterostructures. *J. Appl. Phys.* **1999**, *85*, 3786. [CrossRef]
20. Liu, W.; Li, M.-F.; Chua, S.-J.; Akutsu, N.; Matsumoto, K. Photoreflectance Study of Au-Schottky Contacts on n-GaN. *J. Electron. Mater.* **1999**, *28*, 360. [CrossRef]
21. Hattori, K.; Fukuda, S.; Nishimura, K.; Okamoto, H.; Hamakawa, Y. Interpretation of CPM Measurements in Amorphous Semiconductors. *J. Non-Cryst. Solids* **1993**, *164*, 351. [CrossRef]
22. Kita, T.; Yamada, M.; Wada, O. Dual Chopped Photoreflectance Spectroscopy for Nondestructive Characterization of Semiconductors and Semiconductor Nanostructures. *Rev. Sci. Instrum.* **2008**, *79*, 046110. [CrossRef]
23. Liao, Y.F.; Chang, C.C.; Wang, D.P.; Tseng, B.H.; Liao, Y.D.; Lin, C.H. A Novel Approach for Normalizing the Photoreflectance Spectrum by Using Polymer-Dispersed Liquid Crystal. *Rev. Sci. Instrum.* **2012**, *83*, 103904. [CrossRef] [PubMed]
24. Misiewicz, J.; Sitarek, P.; Sek, G.; Kudrawiec, R. Semiconductor Heterostructures and Device Structures Investigated by Photoreflectance Spectroscopy. *Mater. Sci.* **2003**, *21*, 263.
25. Kobayashi, E.; Shimmura, S.; Ito, S.; Makino, T. A New Photoreflectance Signal Possibly Due to Midgap Interface States in Buried f-Doped SnO2/TiO2 Junctions. *Jpn. J. Appl. Phys* **2019**, *59*, SCCB23. [CrossRef]
26. Zhang, B.; Wang, X.-J. Note: A Modified Optics Based Technique for Suppressing Spurious Signals in Photoreflectance Spectra. *Rev. Sci. Instrum.* **2017**, *88*, 106103. [CrossRef] [PubMed]
27. Ozgur, U.; Alivov, Y.I.; Liu, C.; Teke, A.; Reshchikov, M.A.; Dogan, S.; Avrutin, V.; Cho, S.J.; Morkoc, H. A Comprehensive Review of ZnO Materials and Devices. *J. Appl. Phys.* **2005**, *98*, 041301. [CrossRef]
28. Klingshirn, C. ZnO: From Basics Towards Applications. *Phys. Status Solidi B* **2007**, *244*, 3027. [CrossRef]
29. Ando, M.; Nakayama, M.; Nishimura, H.; Schneider, H.; Fujiwara, K. Franz-Keldysh Oscillations at the Miniband Edge in a GaAs Superlattice. *Superlat. Microstr.* **1997**, *22*, 459. [CrossRef]
30. Makino, T.; Chia, C.H.; Tuan, N.T.; Segawa, Y.; Kawasaki, M.; Ohtomo, A.; Tamura, K.; Koinuma, H. Exciton Spectra in ZnO Epitaxial Layers on Lattice-Matched Substrates Grown with Laser-Molecular-Beam Epitaxy. *Appl. Phys. Lett.* **2000**, *76*, 3549. [CrossRef]
31. Ozaki, S.; Mishima, T.; Adachi, S. Photoreflectance Spectroscopy of ZnO for Ordinary and Extraordinary Rays. *Jpn. J. Appl. Phys* **2003**, *42*, 5465. [CrossRef]
32. Sze, S.M. *Physics of Semiconductor Devices*; Wiley: New York, NY, USA, 1981; ISBN 0471056618.
33. Baenard, W.O.; Myburg, G.; Auret, F.D.; Goodman, S.A.; Meyer, W.E. Metal Contacts to Gallium Arsenide. *J. Electron. Mater.* **1996**, *25*, 1695. [CrossRef]

34. Hall, D.J.; Hosea, T.J.C.; Lancefield, D. Airy Function Analysis of Franz-Keldysh Oscillations in the Photoreflectance Spectra of Layers. *J. Appl. Phys* **1997**, *82*, 3092. [CrossRef]
35. Ashok, S.; Borrego, J.M.; Gutmann, R.J. Electrical Characteristics of GaAs MIS Schottky Diodes. *Solid-State Electron.* **1979**, *22*, 621. [CrossRef]
36. Hughes, P.; Weiss, B.; Hosea, T. Analysis of Franz-Keldysh Oscillations in Photoreflectance Spectra of a GaAs Single-Quantum Well Structure. *J. Appl. Phys.* **1995**, *77*, 6472. [CrossRef]
37. Van Hoof, C.; Deneffe, K.; De Boeck, J.; Arent, D.J.; Borghs, G. Franz-Keldysh Oscillations Originating from a Well-Controlled Electric Field in the GaAs Depletion Region. *Appl. Phys. Lett.* **1989**, *54*, 608. [CrossRef]
38. Mollwo, E. *Semiconductors: Physics of II-VI and i-VII Compounds, Semimagnetic Semiconductors*; Madelung, O., Schulz, M., Weiss, H., Eds.; Landolt-Boernstein New Series; Springer: Berlin/Heidelberg, Germany, 1982; Volume 17, p. 35.
39. Tanguy, C. Analytical Expression of the Complex Dielectric Function for the Hulthe n Potential. *Phys. Rev. B* **1999**, *60*, 10660. [CrossRef]